IOPscience iopscience.iop.org

Home Search Collections Journals About Contact us My IOPscience

High-resolution nonresonant x-ray Raman scattering study on rare earth phosphate nanoparticles

This content has been downloaded from IOPscience. Please scroll down to see the full text.

2015 New J. Phys. 17 043041

(http://iopscience.iop.org/1367-2630/17/4/043041)

View the table of contents for this issue, or go to the journal homepage for more

Download details:

IP Address: 193.205.206.85
This content was downloaded on 22/05/2017 at 17:33

Please note that terms and conditions apply.

You may also be interested in:

Inelastic x-ray scattering in heterostructures: electronic excitations in LaAlO3/SrTiO3
Kari O Ruotsalainen, Christoph J Sahle, Tobias Ritschel et al.

The Ba 4d--4f giant dipole resonance in complex Ba/Si compounds
Ch J Sahle, C Sternemann, H Sternemann et al.

Recent advances in x-ray absorption spectroscopy
Heiko Wende

Hard x-ray emission spectroscopy: a powerful tool for the characterization of magnetic semiconductors
M Rovezzi and P Glatzel

High multipole transitions in NIXS: Valence and hybridization in 4f systems
R. A. Gordon, G. T. Seidler, T. T. Fister et al.

Electronic excitation investigated by IXSS
W Schülke

Electronic structure of (Ga,Mn)As as seen by synchrotron radiation
Kevin Edmonds, Gerrit van der Laan and Giancarlo Panaccione

Low-dimensional systems investigated by x-ray absorption spectroscopy: a selection of 2D, 1D and 0D cases
Lorenzo Mino, Giovanni Agostini, Elisa Borfecchia et al.

New Journal of Physics
The open access journal at the forefront of physics

Deutsche Physikalische Gesellschaft DPG
IOP Institute of Physics

Published in partnership with: Deutsche Physikalische Gesellschaft and the Institute of Physics

CrossMark

OPEN ACCESS

RECEIVED
29 December 2014

REVISED
20 February 2015

ACCEPTED FOR PUBLICATION
25 February 2015

PUBLISHED
20 April 2015

Content from this work may be used under the terms of the Creative Commons Attribution 3.0 licence.

Any further distribution of this work must maintain attribution to the author(s) and the title of the work, journal citation and DOI.

PAPER

High-resolution nonresonant x-ray Raman scattering study on rare earth phosphate nanoparticles

Simo Huotari[1,2], **Edlira Suljoti**[3,4], **Christoph J Sahle**[1,2], **Stephanie Rädel**[4], **Giulio Monaco**[2,5] **and Frank M F de Groot**[3]

[1] Department of Physics, PO Box 64, FI-00014 University of Helsinki, Finland
[2] ESRF - The European Synchrotron, CS40220, 38043 Grenoble Cedex 9, France
[3] Department of Chemistry, Utrecht University, 3584 CA Utrecht, The Netherlands
[4] Helmholtz Center Berlin for Materials and Energy, Albert-Einstein-Str.15, 12489 Berlin, Germany
[5] Department of Physics, University of Trento, Italy

E-mail: simo.huotari@helsinki.fi

Keywords: inelastic x-ray scattering, rare earths, lanthanides, non-dipole, x-ray Raman scattering

Abstract

We report high-resolution x-ray Raman scattering studies of high-order multipole spectra of rare earth $4d \rightarrow 4f$ excitations (the $N_{4,5}$ absorption edge) in nanoparticles of the phosphates $LaPO_4$, $CePO_4$, $PrPO_4$, and $NdPO_4$. We also present corresponding data for La $5p \rightarrow 5d$ excitations (the $O_{2,3}$ edge) in $LaPO_4$. The results are compared with those from calculations by atomic multiplet theory and for the dipole contribution to the La $4d \rightarrow 4f$ transition from a calculation using time-dependent density functional theory (TDLDA). Agreement with the atomic multiplet calculations for the high-order multiplet spectra is remarkable in the case of the $N_{4,5}$ spectra. In contrast, we find that the shallow $O_{2,3}$ semicore excitations in $LaPO_4$ manifest a relatively broad band and an apparent quenching of $5p$ spin-orbit splitting. The more sophisticated TDLDA, which has earlier been found to explain dipolar spectra well in Ba compounds, is less satisfactory here in the case of La.

1. Introduction

Electronic properties of materials are of fundamental interest, as it is well known that understanding electronic properties gives the possibility to tailor the physical, chemical, and biological properties of matter. In wide-band-gap insulators, such as lanthanide phosphate nanoparticles, size-related changes lead to changes in the electronic and geometric structures, i.e., the oxidation state, the crystal phase, or unit cell distortions.

Electronic structures can be studied by various spectroscopic means. The so-called static electron correlation in atomic spectra is the inherent aspect of the many-body problem that couples the motion of the electrons in many-electron atoms and causes the breakdown of the independent electron picture. Interesting phenomena are still being found in atomic spectra, and for example recently it was reported [1] that electron correlation in lanthanide systems coupled to the different radiative and non-radiative decay channels causes a deformation of the inner-shell spectral profiles from a pure Lorentzian in x-ray absorption spectroscopy (XAS) measurements.

A peculiar aspect found in rare earth atomic spectra is the giant dipole resonance (GDR) [2] that prevails in the XAS spectra of, e.g., $4d \rightarrow 4f$ excitations. The GDR spectra have also been studied in detail in compounds other than ones with rare earths since it has been suggested that the GDR shape modulations are sensitive to the local environment of the absorbing atom, yielding novel access to structural information [3, 4]. In rare earths at energies below the GDR, the XAS spectrum typically manifests weak spin-forbidden excitations that gain non-negligible spectral weight due to spin-orbit interaction and the interaction with the GDR. XAS at lanthanide $N_{4,5}$ edges is usually studied with secondary-particle yield techniques due to the very low photon energies involved (~100 eV), which renders transmission-XAS experiments difficult. Recently it has been shown [1] that La $N_{4,5}$ pre-resonances exhibit different XAS spectra in total-electron-yield (TEY) than total-fluorescence-yield (TFY) measurements. The TEY spectra shift to lower energies and in addition show a very asymmetric line profile compared with the symmetric line shape of the TFY spectra. Atomic multiplet calculations have explained this discrepancy by the

© 2015 IOP Publishing Ltd and Deutsche Physikalische Gesellschaft

quantum entangled intermediate states and the interference effects between the different decay channels. In addition, the final states reached in radiative decay are strongly mixed by the $5p$-hole spin-orbit interaction, which modifies the scattering amplitudes of the radiative channels and gives rise to symmetric profiles.

Non-resonant x-ray Raman scattering (XRS) spectroscopy helps to overcome certain challenges related to XAS in the range of low-energy excitations, since it offers true bulk sensitivity and access to liquids [5, 6] and samples contained in complex sample environments such as high-pressure cells [7, 8]. XRS is an energy-loss spectroscopy that provides element-specific information similar to XAS but that uses high-energy x-rays ($\gtrsim$8 keV). In the inelastic scattering process, part of the photon energy is transferred to the electron system and the photon with decreased energy escapes the system and is detected by the experimenter. In the limit of small transferred momentum, the spectra have been shown to be equivalent to those obtained in XAS [9, 10]. One of the differences between the two techniques in practice is that the direction of the momentum transfer vector of XRS takes the role of the polarization vector of XAS, and spectra at high momentum transfers can manifest nondipolar transitions. The information can be used to obtain novel data regarding the electronic structure, hybridization, and ligand field effects of various compounds.

A particular example of recent use of XRS is certain excitations observed in the same energy range as the XAS pre-resonances of lanthanides. They correspond to nondipolar (high-order multipole) excitations that have been also observed in electron energy loss spectroscopy (EELS) [11]. More recently, their existence was also reported in XRS [12, 13]. Gordon *et al* [14] studied them in detail and noted that their contribution became dominant in the XRS spectra of $LaPO_4$ and $CePO_4$ at large exchanged momenta. Since then, high-order multipole spectra of various compounds, including rare earths and actinides [15–18], have been studied. Van der Laan [19, 20] has given a thorough discussion of the corresponding IXS spectra including sum rules.

This article is arranged as follows. After this introduction, methods are presented in section 2, results discussed in section 3, and conclusions presented in section 4. Throughout this article we use atomic units, i.e., $\hbar = m = 1$, except for energies which are given in electron volts (eV).

2. Experimental and computational methods

Inelastic x-ray scattering is a highly useful tool for studying the electronic structure of materials [10]. In the non-resonant process, the measured quantity is the double differential scattering cross section, which can be written in terms of the dynamic structure factor $S(\mathbf{q}, \omega)$,

$$\frac{d^2\sigma}{d\Omega d\omega} = \left(\frac{d\sigma}{d\Omega}\right)_{\mathrm{Th}} S(\mathbf{q}, \omega).$$

Here $\mathbf{q}$ and ω are the momentum and energy, respectively, transferred to the electron system and $(d\sigma/d\Omega)_{\mathrm{Th}}$ is the Thomson scattering cross section. The dynamic structure factor $S(\mathbf{q}, \omega)$ is

$$S(\mathbf{q}, \omega) = \sum_F \left|\langle F|\, e^{i\mathbf{q}\cdot\mathbf{r}}\, |I\rangle\right|^2 \delta\left(\Omega_F - \Omega_I - \omega\right),$$

where $|I\rangle$ and $|F\rangle$ are the initial and final many-electron states, respectively, and Ω_I and Ω_F are their corresponding energies. When the final state $|F\rangle$ involves a hole in a deeply bound core state, the IXS technique is denoted XRS spectroscopy [10]. One of the interesting aspects of XRS compared with many traditional techniques is that the transition operator is an exponential. Expanding this operator using spherical harmonics, it can be seen how in addition to dipolar transitions, higher-order transitions can be observed [21]. XRS spectra manifest dipole transitions at low values of transferred momentum q and thus are similar to those of XAS or EELS. However, at increasing q, higher-order multipoles $k > 1$ begin contributing to the spectra, and one can observe non-dipole transitions. A canonical example is the s-type exciton at the fluorine K edge in LiF, [22] the observation of which requires a technique that can probe $s \rightarrow s$ type transitions. In the absence of excitonic and multiplet effects, the density of unoccupied electron states above the Fermi level is measured. Then the q-dependence of the XRS spectra gives access to the symmetry-projected empty density of states [23].

It has been shown that the q-dependence in XRS is particularly interesting in the lanthanides [14]. In most solid compounds involving La, its oxidation state is La^{3+}, with a $4d^{10}4f^0$ ground state. The term symbol is $^1S_0$. A well-known feature of the $4d \rightarrow 4f$ excitation at the dipole limit is the GDR, [4] which corresponds to a transition $^1S_0 \rightarrow {}^1P_1$. Higher-order multipolar transitions can be observed by EELS and XRS, as thoroughly discussed by Van der Laan [24]. In the LS coupling scheme, transitions are possible for multipoles k that satisfy $|L - L'| < k < |L + L'|$, where L and L' are the angular quantum numbers of the initial and final state configuration, respectively. Together with the requirement that in parity conserving (changing) transitions only even (odd) multipoles are possible, [24] this means that in a $4d \rightarrow 4f$ transition only multipoles of k = 1, 3, and 5 (dipole, octupole, and triakontadipole, respectively) contribute.

The $^1P_1$ state interacts strongly with continuum states, and this mixing gives rise to an asymmetric Fano line shape with a width of 4–5 eV. This seems to be a general feature of transitions with the same principal quantum number in the electron initial and final state (i.e., $nl \rightarrow nl'$). This has been explained by Sen Gupta *et al* [25] to be due to the large electrostatic interaction between the initial and final state wave functions that lifts the dipole term to relatively high energies, where it can interact with the continuum. Unlike the GDR, the high-order multipole transitions are lifted generally much less in energy owing to their higher multipolarity and hence smaller Coulomb integral with the *s*-symmetry ground state. They appear well defined in the spectra, as has been shown by Gordon *et al* [14], and are resolution limited. High energy resolution in their study is desirable, since the spectra are sensitive to the oxidation state of the ion and hybridization. Thus we targeted our study to see how improved energy resolution can help obtain new information from XRS measurements in a rare earth compound.

The measurements were conducted at the beamline ID16 of the European Synchrotron Radiation Facility (ESRF)[6] [36]. The samples we used were powders of $LaPO_4$, $CePO_4$, $PrPO_4$, and $NdPO_4$ nanoparticles with spherelike morphology and 5-nm diameter. The nanoparticles were synthesized by colloidal chemistry, and their surface was passivated by amine chains. The crystallinity, morphology, and size of the particles were investigated using x-ray diffraction and transmission electron microscopy and have been previously reported [26]. In this work, we report x-ray Raman spectra of the $4d \rightarrow 4f$ transitions in $LaPO_4$, $CePO_4$, $PrPO_4$, and $NdPO_4$ (early rare earths with less than half-filled $4f$ shells) nanoparticles as well as a spectrum of the $5d \rightarrow 5p$ transition in $LaPO_4$.

The beam from three consecutive undulators was monochromated using a combination of a Si(111) double-crystal and a Si(333) channel-cut monochromator. The spectra were measured using a nine-element spectrometer designed for high-resolution non-resonant IXS studies [27]. The spectrometer was equipped with seven diced analyzer crystals, and two elastically spherically bent analyzer crystals, all operating in the Johann geometry and employing the Si(nnn) reflection. The Rowland circle diameter, and thus the curvature radii of the analyzers, equaled to 1 m. We used the Si(555) analyzer reflection for $LaPO_4$ and $CePO_4$ samples. The total energy resolution when using the diced analyzer crystals was 180 meV as determined from the quasielastic line width, determined mainly by the incident beam bandwidth. To avoid the strongly excited Lβ fluorescence of Pr and Nd being reflected by the lower-order harmonic Si(333) of the analyzer, $PrPO_4$ and $NdPO_4$ were measured using 13.8 keV using the Si(777) analyzer crystal reflection. This results in a lower absorption cross section and hence a lower fluorescence background. The energy resolution in that case was 280 meV using the diced analyzer crystals. For the diced analyzers, we employed the dispersion compensation algorithm [28, 29]. The total energy resolution when observing data given by the elastically bent analyzer crystals was 1 eV, determined by the bent crystal reflectivity curve [30]. Each analyzer crystal focused the collected radiation onto an individual spot on a Medipix2 hybrid pixel detector [31]. The incident photon energy ω_1 was scanned to obtain the energy-transfer range of 0–125 eV, where the $5d \rightarrow 5p$ and $4d \rightarrow 4f$ transitions of rare earth ions can be observed [14].

Concerning the values of momentum transfer used in this work, one has to take note of the relatively large size of the analyzer array of the spectrometer [27]. For a given value of mean scattering angle 2θ of the spectrometer ensemble, the two elastically bent crystals were situated at the scattering angles $2\theta - 13° \pm 2.3°$ and $2\theta - 6.5° \pm 2.3°$. The uncertainties are due to the finite size of each analyzer crystal, yielding a finite momentum transfer resolution. The seven diced analyzer crystals were located so that one analyzer had an angle of $2\theta - 6.5°$; two of them, 2θ; the next two, $2\theta + 6.5°$; and finally the last two, $2\theta + 13°$. Each had the same angular opening, $\pm 2.3°$. For this reason, the 1-eV resolution data recorded using the elastically bent crystals shown later in this article, are taken at slightly lower momentum transfer values than the high-resolution data taken with the diced analyzers.

The measurements were done at two values of 2θ, namely, 45° and 134°. For the low-momentum transfer setting that was used in the case of La $4d \rightarrow 4f$, this yields the individual momentum transfer values 2.7, 3.3, 3.9, 4.4, and 4.9 $Å^{-1}$, with uncertainties of ± 0.2 $Å^{-1}$, for each value. For the high-momentum transfer setting for La and Ce, the corresponding values are 8.8, 9.0, 9.3, 9.5, and 9.7 $Å^{-1}$, with uncertainties of ± 0.1 $Å^{-1}$. Similarly, for the high-momentum transfer setting for Pr and Nd, owing to the higher analyzer energy, the momentum transfers were 12.3, 12.6, 13.0, 13.3, and 13.5 $Å^{-1}$ (± 0.1 $Å^{-1}$). For La and Ce, we will thus refer to the mean momentum transfer values of 3.0 $Å^{-1}$ and 8.9 $Å^{-1}$ for the low-resolution data and 4.2 $Å^{-1}$ and 9.4 $Å^{-1}$ for the high-resolution data unless otherwise specified. For Pr and Nd, we discuss only the high-energy-resolution measurement done using the high-momentum transfer setting, and then the mean value comes to $q = 13$ $Å^{-1}$.

[6] The inelastic x-ray scattering beamline ID16 was closed in 2012, replaced by a new beamline ID20 that has been recently constructed as a part of the ESRF Upgrade Program Phase I.

The experimental results for the nondipolar transitions are compared with results from atomic multiplet code by Cowan [32] in intermediate coupling, assuming rare earth ions in spherical symmetry. The calculations were done in the Hartree–Fock approximation with relativistic corrections. The Slater–Condon parameters were scaled to 80% of their atomic values to account for correlation and screening (represented by a scaling parameter $g = 0.8$). For the calculation of the the $N_{4,5}$ multipole spectra the Hartree–Fock value for the spin–orbit interaction was used. As will be seen, the La^{3+} $O_{2,3}$ spectra were found to be in better agreement with the experiment when the $5p$ spin–orbit interaction was adjusted to 70% of its atomic value (represented by a scaling parameter $z = 0.7$). Multiplet calculations were done for each individual analyzer q value, and the obtained spectra were averaged over the analyzer array to simulate the experimental solid angle spread function as precisely as possible.

The GDR features are known to exhibit much larger bandwidth than the multipolar spectra and are not adequately explained by the atomic multiplet approach. The dipolar spectrum for La was modeled using the real space multiple scattering (RSMS) approach, using the FEFF code [33] within the time-dependent local density approximation (TDLDA) to account for collective phenomena. This method has worked well for barite ($BaSO_4$) [13] and for complex Ba/Si compounds [4].

3. Results

3.1. La $4d \rightarrow 4f$

The La $N_{4,5}$ edge ($4d \rightarrow 4f$) XRS spectra were measured for the two momentum transfer regimes as described in the preceding section. Figure 1 shows the results for the smaller q value. The lower momentum transfer makes it possible to probe simultaneously the dipole and octupole transitions, i.e., the $^1P_1$ peak and the $^3F_3$, $^1F_3$, and weak $^3D_3$ peaks (figure 1 upper panel). It should be noted that these are different transitions from the pre-resonances seen in XAS, due to different selection rules. In the dipole limit weak pre-resonances of $^3P_1$ and $^3D_1$ are known to be measurable by XAS. They would be nominally forbidden spin-flip transitions but gain spectral weight owing to the spin-orbit coupling that mixes the states. The same phenomenon is seen in the high-order multipole XRS spectra. In principle the $^3P_1$ and $^3D_1$ excitations would appear in the low-q XRS spectrum as well but are too weak to be observed within the statistics. Moreover, they are partially masked by the high-order multipole excitations, which are relatively strong in the XRS spectra, even at the lowest q shown here.

It can be seen that the $^1P_1$ peak is greatly broadened in experiment, as is known for the GDR. To model this phenomenologically, a Fano line shape is typically used [24]. For the GDR in Ba, the TDLDA approach within the FEFF code has been successfully used [4, 13]. Encouraged by the results for Ba, we also performed a TDLDA calculation for La $4d \rightarrow 4f$ transition, with the results shown in figure 1. The details of the calculations are the same as used in the Ba case. However, in this case TDLDA greatly overestimates the line width. Although the GDR breadth is on the order of 20–30 eV, in La it is less than 10 eV. However, TDLDA predicts a result that is comparable to that for Ba (a band that has an ~20-eV width). This discrepancy is intriguing and deserves further investigation.

Concerning the line shape of the high-order multipole excitations, the $^3F_3$ peak appears symmetric with our experimental resolution of 180 meV. This is demonstrated in the zoom-up in the lower panel of figure 1. This is in contrast with the $^3D_1$ peak measured by TEY, which exhibits an asymmetric shape [1]. The asymmetry of the $^3D_1$ excitation spectral shape for TEY in [1] is due to the intereference of the discrete $^3D_1$ final state and the continuum (i.e., the tail of the $^1P_1$ excitation). This interference is strong because of the same value, $J = 1$, for the two excited states and due to the similar oscillator strengths of $^1P_1$ and $^3D_1$ at the pre-resonance energy. In the case of our XRS spectra, the different J values and the predominant oscillator strength of the multipolar $^3F_3$ excitation lead to negligible interference and hence symmetric non-dipole peaks. The line width of the multipole peaks is ~300 meV, measured with 180-meV resolution. The spectra are thus not resolution limited. Thus, the intrinsic width is on the order of 240 meV if we assume Gaussian lineshapes.

Figure 2 shows the experiment and theory focused on the high-order multipole region measured with an energy resolution of 180 meV for the two momentum transfers. The triakontadipole ($k = 5$) transitions with the final states with $^3H_5$, $^3G_5$ and $^1H_5$ term symbols are barely visible in the low-q spectrum but become strong when the momentum transfer, q, is increased. The agreement between experiment and the multiplet theory is remarkable. As discussed hereafter, the momentum transfer dependence of the spectra depends on the radial wave functions, which in the calculation were taken to be the atomic Hartree–Fock functions. In a real solid-state system they can be slightly different from the free-ion case, which may give rise to a discrepancy between experiment and theory concerning the relative weight of $k = 3$ and $k = 5$ transitions. This is manifested in this case in figure 2, which shows that an effective momentum transfer increase of ~10% in both cases would fit the experimental result better. This is clearly seen in the high-q case (experiment at 9.4 $Å^{-1}$) owing to the high

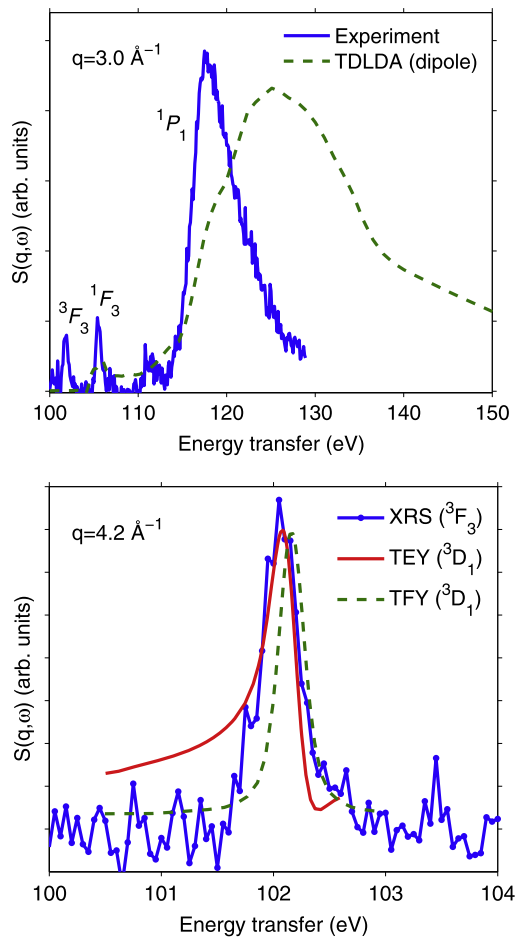

Figure 1. Upper panel: $LaPO_4$ $4d \rightarrow 4f$ spectra, measured with 1-eV energy resolution. The giant dipole resonance dominates the experimental spectrum, with weak multipolar features (pre-resonances) at lower energies. The experimental result is compared with a TDLDA computation. Lower panel: the $^3F_3$ peak seen closer with 180-meV resolution, to observe its inherent line shape, compared with the dipolar $^3D_1$ peak measured with TEY and TFY XAS (taken from [1]).

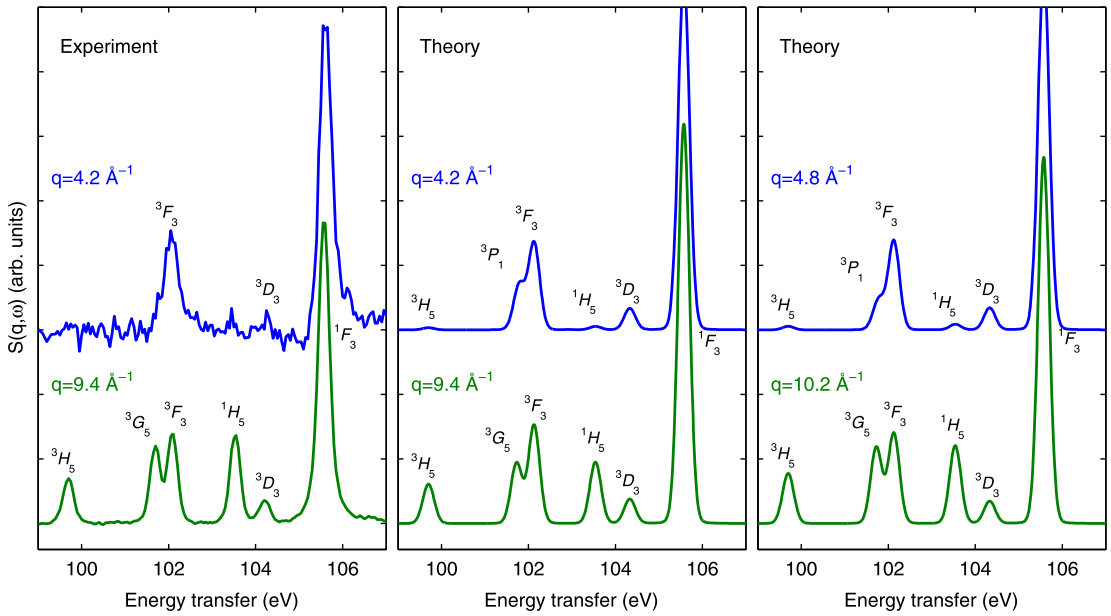

Figure 2. La $4d \rightarrow 4f$ pre-resonance region of $LaPO_4$ measured with180-meV resolution. Also shown are atomic multiplet theory results for the experimental momentum transfer and for a higher momentum transfer that fits the experimental result better.

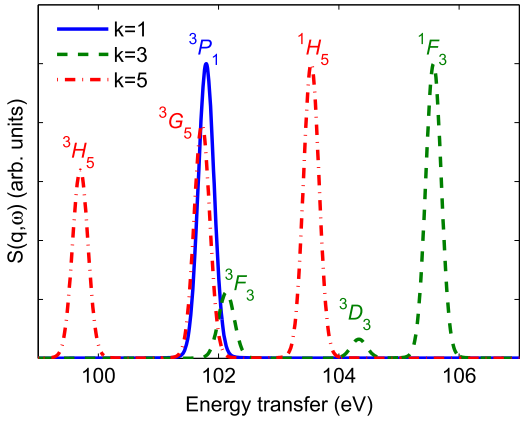

Figure 3. Different multipolar components of the spectra seen in figure 2. The spectra have been normalized to the maximum of each multipole spectrum.

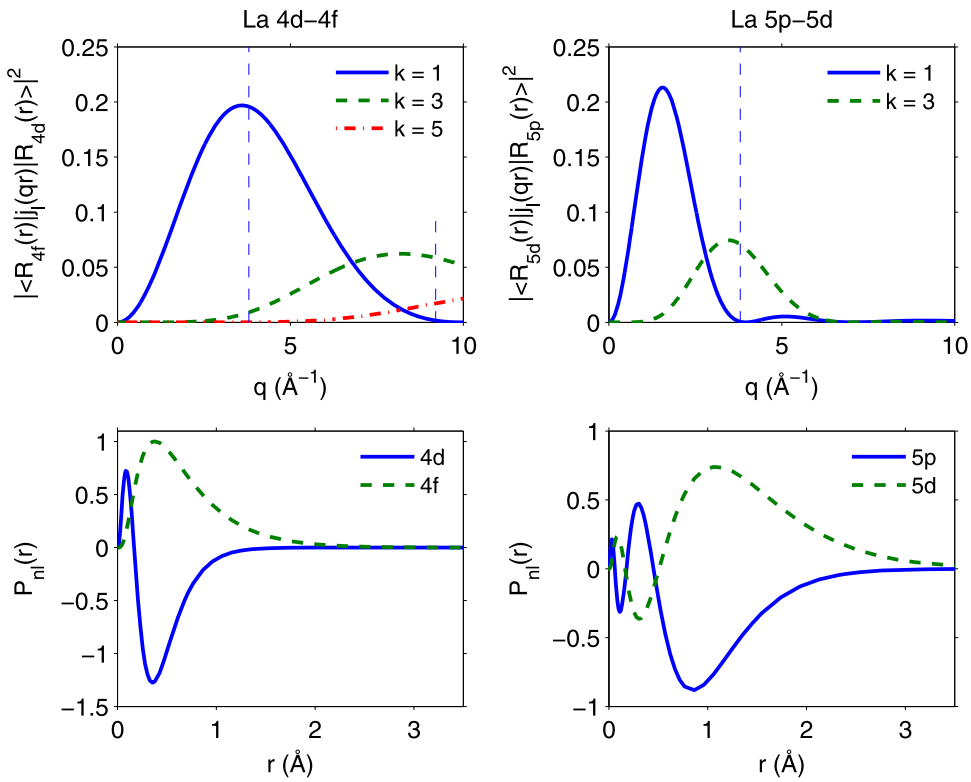

Figure 4. Upper panel: the expectation values of spherical Bessel functions of rank $k = 1$–3 for the La $4d \rightarrow 4f$ (left) and $5p \rightarrow 5d$ (right) transitions. The dashed vertical lines denote the values of momentum transfer at which the measurements were performed. Lower panel: radial probability density of the $4d$ and $4f$ (left) as well as the $5p$ and $5d$ (right) wave functions.

statistical accuracy of the measured spectra. Figure 3 shows the breakdown of the spectra into the components $k = 1, 3$, and 5.

Figure 4 shows the q dependence of different multipolar excitations for the La $4d \rightarrow 4f$ and $5p \rightarrow 5d$ transitions, assuming atomic Hartree–Fock wave functions. The experimental momentum transfer values are shown as dashed vertical lines. For the $4d \rightarrow 4f$ excitation, the momentum transfers correspond to the maximum of the dipole and to an approximate maximum of the higher-order multipoles. For the $5p \rightarrow 5d$ transition, discussed in the next subsection, we concentrated on the maximum of the octupole (the only allowed high-order multipole) excitations. Due to the larger spatial extents of the $5p$ and $5d$ shells compared with those of the $4p$ and $4f$ shells, both dipolar and octupolar $5p \rightarrow 5d$ excitations exhibit expected intensity maxima at considerably lower momentum transfers than they do in the $4d \rightarrow 4f$ transitions. The calculation has been done for the free La^{3+} ion, so one might expect a certain amount of deviation from these results in a real solid-

state system. Bradley *et al* [16] have shown that in the case of Ce, the q-dependence predicted by Cowan's atomic code is in good agreement with the experiment. In our case, we see that the relative strength of the octupole versus triakontadipole transitions needs finally to be slightly scaled to match the experiment in figure 2. This is manifested by better agreement with experiment if slightly higher values of q are used in the theory. This may be owing to a slight but discernible modification of the radial wave function in the solid state as compared with the pure ionic one.

3.2. La $5p \rightarrow 5d$

We investigated the $O_{2,3}$ edges, i.e., the $5p \rightarrow 5d$ excitations, of La in $LaPO_4$, with momentum transfer of 4.2 $Å^{-1}$. The observed transitions obey the triangle rule $1 \leqslant k \leqslant 3$, so only dipolar and octupolar transitions could in principle be observed. As seen in figure 4, the momentum transfer used here corresponds to the maximum for the octupolar transition, with the dipole transitions strongly suppressed.

The corresponding experimental and theoretical spectra are shown in figure 5. The agreement between experiment and atomic multiplet theory here is not as perfect as it is for the $N_{4,5}$ edges. First of all, the O shell, being a relatively low-lying semicore shell, interacts strongly with the valence electrons such that the spectrum is broadened into a band with an ~0.5-eV bandwidth. In contrast with the very localized character of the $4f$ orbitals, the $5d$ orbitals have a larger radial extent (see figure 5) and are strongly mixed with oxygen $2p$ and phosphor $3p$ orbitals [26]. In addition, the presence of a multitude of different surface states with differing energies causes an additional broadening of the valence spectral structures. Therefore, to obtain reasonable agreement with the experiment, the spectrum from the multiplet calculation had to be given a 0.5-eV Lorentzian bandwidth. This suggests that the $5p \rightarrow 5d$ semicore excitations are more sensitive to solid-state effects than the $4d \rightarrow 4f$ excitations.

When the Hartree–Fock value for the $5d$ spin-orbit interaction is used ($z = 1.0$), the multiplet theory also overestimates the peak splitting. This can be an indication of a quenching of the $5d$ spin-orbit interaction in $LaPO_4$ as compared with the free La^{3+} ion, rendering the spectra more toward the LS coupling scheme. This is shown in figure 5 , which presents multiplet calculations using two different values for scaling of the spin-orbit coupling. The effect of systematic scaling of the Slater–Condon integrals (g) and of the spin-orbit interaction (z) is shown in figure 5 as well. The best agreement is obtained by using $g = 0.8$ and $z = 0.7$ in addition to the spectral broadening by 0.5 eV as previously described. However, the high-energy shoulder at ~24 eV remains unexplained. Overall, based on these results one may argue that the $O_{2,3}$ spectra in $LaPO_4$ can show different behavior than the $N_{4,5}$ spectra due to the higher sensitivity to local structure. It would be interesting to study the semicore excitation spectra in this class of systems (e.g., bulk versus nanoparticles) more closely using XRS [34, 35]. For instance, oxygen K-edge XAS spectra of the entire lanthanide series have revealed particle-size effects on the oxygen–lanthanide covalent bonding [26].

One should additionally consider the effect of the crystal field on the $5d$ states in the description of the spectra. In $LaPO_4$, the La^{3+} ions are nine-fold coordinated by nearest-neighbor oxygen ions, resulting in a relatively spherical crystal field. However, the crystal field will mix states with different values of J. In Ce systems (e.g., CeO_2), the crystal field parameter $10Dq \sim 2$ eV, which should have a noticable effect on the spectra. However, the nine-fold coordination would complicate the analysis in the case of $LaPO_4$ considerably. Indeed, our calculations (not shown) for octahedral and tetrahedral crystal fields do not tend to improve the agreement between experiment and theory.

3.3. Ce, Pr and Nd $4d \rightarrow 4f$

For $CePO_4$, $PrPO_4$, and $NdPO_4$, we measured the $4d \rightarrow 4f$ transitions only at a large momentum transfer setting for the high-order multipoles, thus including octupole and triakontadipole transitions.

Although in the case of the La^{3+} $N_{4,5}$ edges there are four octupole transitions (only three being visible for practical purposes, a $^3D_3$ excitation at 100.7 eV being much weaker than the others) and three triakontadipole ones, the progressively filling $4f$ shell renders the spectra of Ce, Pr, and Nd much more complex. There are, all told, 91 octupole and 82 triakontadipole transitions in Ce^{3+}, 337 octupole and 367 triakontadipole transitions in Pr^{3+}, and finally 822 octupole and 954 triakontadipole transitions in Nd^{3+}. The spectra were calculated using the Hartree–Fock Slater–Condon parameters with scalings of $g = 0.8$ and $z = 1.0$. The increasing complexity is seen clearly in the high-resolution data sets of figure 6. Agreement between the experiment and the atomic multiplet calculations is remarkable, indicating that in these systems solid-state effects do not affect the spectra greatly in these cases. However, as shown by Gordon *et al* [14], increasing hybridization, as in $CeRh_3$, will have a profound effect on the spectra. Within the high sensitivity of this high-resolution experiment, for the series of phosphates studied here, the $N_{4,5}$ multipole spectra do not show such effects, unlike the $O_{2,3}$ edge of La in $LaPO_4$. We found that a similar scaling of the effective q in the multiplet calculation, demonstrated to improve the agreement between theory and experiment in La (figure 2), does not have a remarkable effect on the agreement for Ce, Pr, or Nd, where the agreement is already very good when the nominal value of q is used (figure 6).

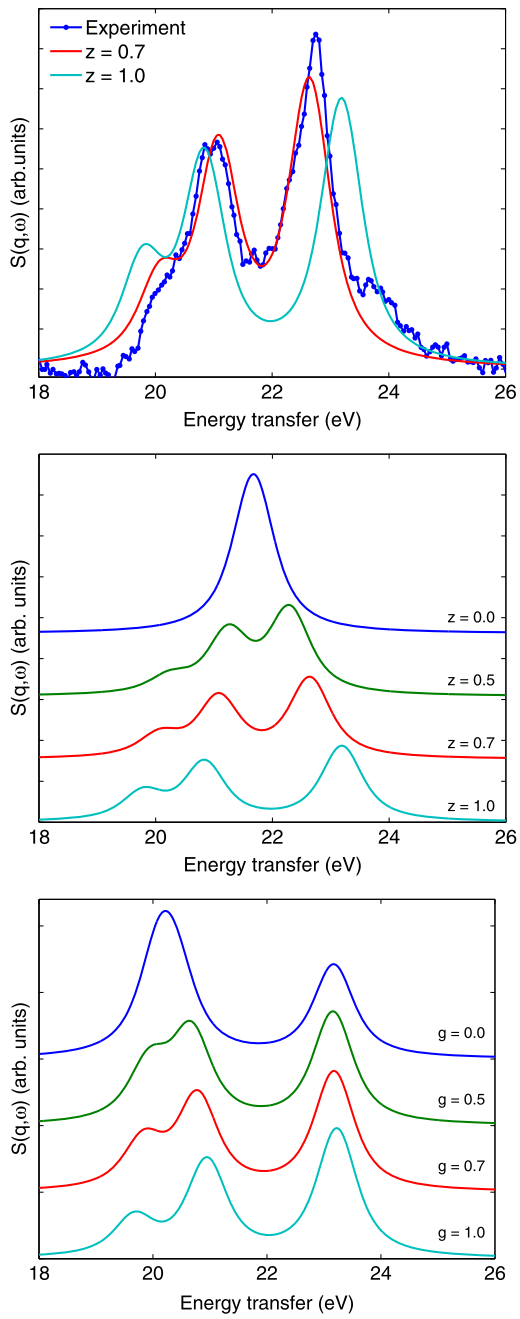

Figure 5. Upper panel: La $5p \rightarrow 5d$ spectra from experiment and best-fitted theory. The spectrum manifests octupolar transitions. The Slater–Condon integrals have been scaled to 80% ($g = 0.8$). Spectra have been calculated using two values for $5d$ spin-orbit interaction ζ_{5d}: for the Hartree–Fock value ($z = 1.0$) and the value scaled by 70% ($z = 0.7$). Middle panel: corresponding spectra calculated by varying z between 0 (pure LS coupling) and 1, using $g = 0.8$. Lower panel: corresponding spectra calculated by varying g between 0 (pure jj-coupling) and 1, using $z = 1.0$. In the middle and lower the panels, the spectra have been offset vertically for clarity.

The crystal field effects in $4d \rightarrow 4f$ spectra of rare earths are small (<50 meV) and cannot be seen directly in the spectral shapes. However, the multipole spectra depend strongly on the ground-state value of J, and the crystal field can mix states with different J. This mixing effect is seen, e.g., in resonant IXS spectra [36] since it allows final states that would be otherwise forbidden. Such mixing effects are not greatly manifested in our XRS spectra since neglecting crystal field effects is found to produce good agreement with experiment.

4. Conclusions

We report high-resolution measurements of the $4d \rightarrow 4f$ transitions of the rare earth ion (the $N_{4,5}$ absorption edge) in $LaPO_4$, $CePO_4$, $PrPO_4$, and $NdPO_4$. We also report $5p \rightarrow 5d$ transitions (the $O_{2,3}$ edge) in $LaPO_4$. The method chosen was high energy resolution XRS spectroscopy. The experimental results are compared with those

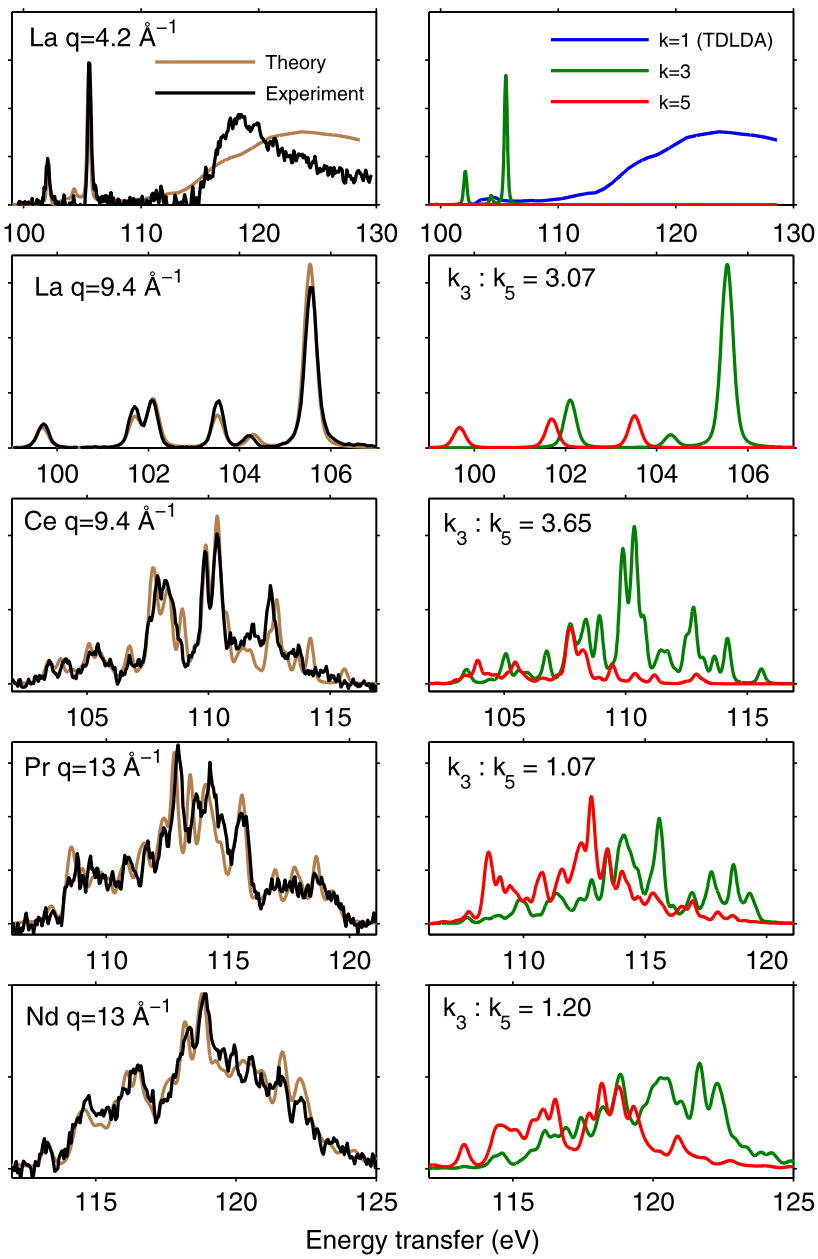

Figure 6. The $4d \rightarrow 4f$ excitations, La to Nd. For La, two momentum transfer values are shown; for others, only a large momentum transfer setting was used in order to focus on the high-order multipolar transitions. Left panels: experiment and theory. Right panels: theory decomposed to different multipolar components ($k = 1, 3, 5$). The relative weights between the components $k = 3$ and $k = 5$ are indicated.

from calculations by atomic multiplet theory using Cowan's code and, for the dipole spectrum, of $LaPO_4$ from a calculation using TDLDA with the FEFF code.

Agreement with the atomic multiplet calculations for the non-dipolar spectra is remarkable in the case of the $4d \rightarrow 4f$ transitions, owing to the localized atomic character of the $4f$ orbitals. For the non-dipolar shallow $5p \rightarrow 5d$ semicore excitation in $LaPO_4$, the agreement between experiment and atomic multiplet theory is not excellent because the $5d$ (possibly also $5p$) shell is influenced by solid-state effects and we observe an apparent quenching of the $5p$ spin-orbit interaction. The high-order multipole spectra have indeed a capability to yield novel information about the electronic structure of rare earth compounds, and these observed effects deserve more studies to be completely understood.

Interestingly TDLDA, which has earlier been shown to work well in the case of complex Ba compounds in explaining the dipolar $4d \rightarrow 4f$ excitation [4, 13], works less well here in the case of La. This is seen as the calculation yielding a broader line shape than is observed in the experiment. This opens up the question of the nature of the giant dipole resonance; why it behaves differently in lanthanides than in barites remains as well an open question for future studies.

These results give a systematic and detailed perspective of the electronic spectra of these compounds, especially in the case of the non-dipolar excitations that we have studied with higher resolving power than has been attainable before.

Acknowledgments

Beam time was granted by the European Synchrotron Radiation Facility. Funding was provided by the Academy of Finland (Grants 1283136, 1256211, 1127462, and 1259526) and the University of Helsinki Research Funds (Grant 490076). We are grateful to C Henriquet, M-C Lagier, and the entire beamline ID16 team and support groups for expert assistance, advice, and encouragement during the experiment. We thank S Heinäsmäki and M Hakala for invaluable discussions.

References

[1] Suljoti E, de Groot F M F, Nagasono M, Glatzel P, Hennies F, Deppe M, Pietzsch A, Sonntag B, Föhlisch A F and Wurth W 2009 *Phys. Rev. Lett.* **103** 137401
[2] Dehmer J L, Starace A F, Fano U, Sugar J and Cooper J W 1971 *Phys. Rev. Lett* **26** 1521
[3] Phaneuf R A *et al* 2013 *Phys. Rev.* A **88** 053402
[4] Sahle C *et al* 2014 *J. Phys. B: At., Molec. Opt. Phys.* **47** 045102
[5] Wernet P *et al* 2004 *Science* **304** 995
[6] Conrad H, Lehmkühler F, Sternemann C, Sakko A, Paschek D, Simonelli L, Huotari S, Feroughi O, Tolan M and Hämäläinen K 2009 *Phys. Rev. Lett.* **103** 218301
[7] Sahle C J *et al* 2013 *Proc. Natl Acad. Sci. USA* **110** 6301
[8] Pylkkänen T, Giordano V M, Chervin J C, Sakko A, Hakala M, Soininen J A, Hämäläinen K, Monaco G and Huotari S 2010 *J. Phys. Chem.* B **114** 3804
[9] Mizuno Y and Ohmura Y 1967 *J. Phys. Soc. Jpn* **22** 445
[10] Schülke W 2007 *Electron Dynamics Studied by Inelastic X-ray Scattering* (Oxford: Oxford University Press)
[11] Netzer F P, Strasser G and Matthew J A D 1983 *Phys. Rev. Lett.* **51** 211
[12] Sternemann C, Soinnen J A, Vankó G, Volmer M, Secco R A, Tolan M and Tse J S 2005 *Phys. Rev.* B **72** 035104
[13] Sternemann C, Sternemann H, Huotari S, Lehmkühler F, Tolan M and Tse J S 2008 *J. Anal. At. Spectrom.* **23** 807
[14] Gordon R A, Seidler G T, Fister T T, Haverkort M W, Sawatzky G A, Tanaka A and Sham T K 2008 *EPL* **81** 26004
[15] Willers T *et al* 2012 *Phys. Rev. Lett.* **109** 046401
[16] Bradley J A, Moore K T, van der Laan G, Bradley J P and Gordon R A 2011 *Phys. Rev.* B **84** 205105
[17] Caciuffo R, van der Laan G, Simonelli L, Vitova T, Mazzoli C, Denecke M A and Lander G H 2010 *Phys. Rev.* B **81** 195104
[18] Bradley J A, Gupta S S, Seidler G T, Moore K T, Haverkort M W, Sawatzky G A, Conradson S D, Clark D L, Kozimor S A and Boland K S 2010 *Phys. Rev.* B **81** 193104
[19] van der Laan G 2012a *Phys. Rev. Lett.* **108** 077401
[20] van der Laan G 2012b *Phys. Rev.* B **86** 035138
[21] Soininen J A, Ankudinov A L and Rehr J J 2005 *Phys. Rev.* B **72** 045136
[22] Hämäläinen K, Galambosi S, Soininen J A, Shirley E L, Rueff J-P and Shukla A 2002 *Phys. Rev.* B **65** 155111
[23] Mattila A, Soininen J A, Galambosi S, Huotari S, Vankó G, Zhigadlo N D, Karpinski J and Hämäläinen K 2005 *Phys. Rev. Lett.* **94** 247003
[24] van der Laan G 2012c *Phys. Rev.* B **86** 035138
[25] Sen Gupta S, Bradley J A, Haverkort M W, Seidler G T, Tanaka A and Sawatzky G A 2011 *Phys. Rev.* B **84** 075134
[26] Suljoti E, Nagasono M, Pietzsch A, Hickmann K, Trots D M, Haase M, Wurth W and Föhlisch A 2008 *J. Chem. Phys.* **128** 134706
[27] Verbeni R, Pylkkänen T, Huotari S, Simonelli L, Vankó G, Martel K, Henriquet C and Monaco G 2009 *J. Synchrotron Radiat.* **16** 469
[28] Huotari S, Vankó G, Albergamo F, Ponchut C, Graafsma H, Henriquet C, Verbeni R and Monaco G 2005 *J. Synchrotron Radiat.* **12** 467
[29] Huotari S, Albergamo F, Vankó G, Verbeni R and Monaco G 2006 *Rev. Sci. Instrum.* **77** 053102
[30] Honkanen A-P, Verbeni R, Simonelli L, Moretti Sala M, Monaco G and Huotari S 2014 *J. Synchrotron Radiat.* **21** 104
[31] Llopart X, Campbell M, Dinapoli R, Segundo D S and Pernigotti E 2002 *IEEE Trans. Nucl. Sci.* **49** 2279
[32] Cowan R D 1981 *The Theory of Atomic Structure and Spectra* (Berkeley: University of California Press)
[33] Ankudinov A, Nesvizhskii A and Rehr J 2003 *Phys. Rev.* B **67** 115120
[34] Huotari S, Soininen J A, Vankó G, Monaco G and Olevano V 2010 *Phys. Rev.* B **82** 064514
[35] Ruotsalainen K O, Hakala M, Sahle C J, Hämäläinen K, Fister T T, Gordon R A and Huotari S 2014 in preparation
[36] Butorin S 2000 *J. El. Spectr. Rel. Phen.* **110-111** 213